



# Study of the generation of shocks by high-speed jets using conditional averaging

Pierre Pineau\* and Christophe Bogey†

*Univ Lyon, École Centrale de Lyon*

*Laboratoire de Mécanique des Fluides et d'Acoustique*

*LMFA, UMR CNRS 5509*

*69134, Écully, France*

Two isothermal jets and one heated jets at acoustic Mach numbers of 2 and at Reynolds numbers of 12,500 and 50,000 are computed by Large-Eddy Simulation (LES) with the aim of investigating the formation of shocks associated with the perception of crackle. The LES are performed using high-order finite differences on grids containing approximately 300M points. The main properties of the flow and acoustic fields are characterized by mean of instantaneous representations and time-averaged statistics. Notably, steep sound waves possessing the distinctive features of crackle are observed close to the jets, leading to significant levels of skewness in the pressure and dilatation fields. The steepened aspect of these waves is already pronounced in the near vicinity of the turbulent flow, which suggests that it is mainly the result of a source mechanism. In order to educe this source mechanism, a conditional averaging method is applied to isolate the strongest pressure waves from the rest of the signal, and to determine the most salient features of their generation process. In particular, it is found that these waves originate from the turbulent flow as straight, inclined wavefronts, and that their generation process is linked to the supersonic convection of large-scale coherent structures inside the jet shear layers.

## I. Introduction

In the last decades, the presence of steep, jagged shock structures has been reported in the far acoustic fields of high-speed supersonic jets issued from model scale nozzles<sup>1-3</sup> as well as full-scale military jet engines.<sup>4</sup> These shocks occur primarily in the aft quadrant of the jets and are believed to be the cause of an unpleasant perception effect known as crackle noise.<sup>5</sup> Despite several years of research, the process by which they are formed is still not fully understood. Indeed, different mechanisms can lead to the formation of shocks in the sound field produced by such highly compressible flows. Notably, it is well established that the sound waves they generate are strong enough to be affected by nonlinear distortions.<sup>6,7</sup> These nonlinear effects cumulate during propagation, leading to the progressive formation of shocks, as observed in measurements performed in the acoustic far fields of military jet aircrafts,<sup>8</sup> as well as in numerical simulations.<sup>9</sup> However, estimations of the propagation distances required for shock formation have shown that, in some cases, steepened waveforms were found too close from the jet to be only the result of nonlinear propagation effects.<sup>5,10,11</sup> This is particularly true in the case of jets exhausting from small-scale nozzles in range-restricted environments.<sup>11,12</sup> For these jets, the peak frequencies are higher than in full-scale tests and the effects of molecular absorption, which counteracts the formation of shocks, are thus stronger. In order to account for the presence of shocks in these experiments, it has been suggested<sup>2,5</sup> that the steepened aspect of the waveforms was, at least to some extent, the consequence of a source mechanism located inside the jet. The possibility of shock formation at the source, in the vicinity of the turbulent flow, has been confirmed by optical visualization<sup>13,14</sup> and numerical simulations<sup>15-17</sup> of jets and mixing layers. In these studies, shocks are found emerging from the shear layers, suggesting that they are caused by events occurring inside the flow.

\*PhD student, pierre.pineau@doctorant.ec-lyon.fr.

†CNRS Research Scientist, AIAA Senior Member & Associate Fellow, christophe.bogey@ec-lyon.fr

As observed in the simulations of Buchta & Freund,<sup>18</sup> as well as in the experimental measurements of Fiévet et al.,<sup>19</sup> these shocks merge with each others and steepen as they propagate in the downstream direction, leading to fewer and stronger waves<sup>18,19</sup> with increasing distance from the jet. The waves resulting from this source mechanism are expected to play a key role in the formation of crackle in the far field. Indeed, passive noise reduction devices such as chevrons or nozzle inserts have been observed to significantly alter the crackling behaviour of the sound field produced by model and full-scale supersonic jets.<sup>13,20</sup> Since these control methods act upon the structure of the near-nozzle turbulent flow, it is likely that the steepened aspect of the wavefronts is already present, at least partly, at the time of their formation inside the turbulent flow. Despite their importance, the mechanisms by which shocks are produced inside the jets shear layers are not well understood. In particular, an important question concerns the role of coherent structures in their formation process. Large-scale coherent structures are known to play a key role in the generation of sound by high-speed jets.<sup>21,22</sup> When convected at supersonic velocities, they generate Mach waves<sup>23-25</sup> that contribute to a major part of the sound radiated in the downstream direction, where the perception of crackle is most intense. The mechanisms at the origin of Mach waves are now reasonably well understood thanks, notably, to previous studies describing this phenomenon in a linear framework.<sup>24-26</sup> In particular, linear models have allowed the prediction of several aspects of Mach waves, such as the direction of maximum noise emission, or the shape of the spectra near the peak frequency.<sup>26,27</sup> In these approaches, coherent structures are modeled as linear instability waves with supersonic phase velocities which radiate sound in the far field by a mechanism analogous to the generation of sound by a supersonic flow over a wavy wall. Obviously, the formation of shocks is excluded in the case of such linear models, since the predicted waveforms consist of smooth, harmonic waves. Nevertheless, it is legitimate to wonder whether the steepened waves observed near the jets in optical visualizations and numerical simulations constitute an extreme case of Mach waves, for which flow perturbations are too strong to be accurately described by linear theory. If so, a better knowledge of the properties of coherent structures at the origin of Mach waves should allow us to shed some light on the source mechanisms responsible for shock formation.

In the present study, Large Eddy Simulations (LES) of three isothermal and heated jets at an acoustic Mach number of 2 are carried out in order to examine the mechanisms responsible for the formation of shocks in the near acoustic field. In particular, the objective is to investigate how they can be linked to the generation of Mach waves by coherent structures inside the jet flow. More specifically, two isothermal jets at diameter-based Reynolds numbers of 12,500 and 50,000 are first computed given that previously, studying the variations of sound sources with this parameter has helped to highlight the role of coherent structures<sup>23,28,29</sup> in noise generation. Indeed, when the Reynold number is decreased, the scales affected by molecular viscosity become larger, and coherent structures are thus easier to detect and study, while the dominant noise generation mechanisms remain representative of those observed in jets at high-Reynolds number.<sup>28</sup> In order to complete this database, a heated jet at an acoustic Mach number of 2.06 and at a Reynolds number of 50,000 is also computed with the aim of investigating how a rise in temperature can affect the formation of shocks. The exhaust velocities of the jets are well above the ambient speed of sound, and the generation of Mach waves and crackle noise is thus expected, according to previous experimental<sup>5,30,31</sup> and numerical studies<sup>32</sup> of jets at comparable acoustic Mach numbers. Unfortunately, coherent structures are difficult to define and detect using conventional metrics, such as time averaged statistics and spectra. In the past, methods based on conditional averages have been successful in educing the most general features of these structures in turbulent jets,<sup>33,34</sup> and boundary layers.<sup>35</sup> These methods consist in synchronizing several flow events over a trigger condition. The synchronized events are then ensemble averaged such that only generic, coherent features remain, while incoherent, uncorrelated information fade away as background noise. In the present study, conditional averages are computed from the flow and sound fields of the three present simulations in order to describe how the strongest sound waves in the near field can be related to flow events and, in particular, to the motion of coherent structures inside the jets.

The paper is organized as follows: First the numerical methods and main parameters of the LES are introduced. The main characteristics of the flow and acoustic fields of the jets are then presented. They include mean and instantaneous representations, as well as spectra of the near-field pressure fluctuations. Next, the presence of steepened waves in the near acoustic field is examined, and their properties are quantified using time averaged high-order statistics. Individual shocks are then extracted from the pressure fluctuations signals and their properties are discussed using a conditional averaging method. Last, conditional averages are applied to the jet flow and sound fields in order to characterize the generation of a mean shock-event.

## II. Numerical methodology

### II.A. Jet parameters

Two isothermal and one heated supersonic jets are simulated in the present study. The two isothermal jets are at Mach numbers  $M_j = u_j/a_j$  of 2 and at diameter-based Reynolds numbers  $Re_D = u_j D/\nu$  of 12,500 and 50,000, where  $u_j$  is the jet exhaust velocity,  $a_j$  is the speed of sound inside the jet,  $D = 2r_0$  is the jet diameter, and  $\nu$  is the kinematic viscosity. They are labeled IsoRe12500 and IsoRe50000, respectively. The heated jet is at  $M_j = 1.5$  and at a Reynolds number of 50,000, and is referred to as HotRe50000. The temperature ratio  $T_j/T_\infty$  of this jet is equal to 1.87, where  $T_j$  is the jet static temperature and  $T_\infty = 293$  K is the temperature of the ambient medium. This temperature ratio yields an acoustic Mach number  $M_a = u_j/a_\infty$  of 2.06, where  $a_\infty$  is the ambient speed of sound, which is very close to the acoustic Mach numbers of the isothermal jets. Moreover, the exhaust conditions of this heated jet have been chosen in order to match those of a heat-simulated helium jet investigated by Papamoschou & Debiasi.<sup>31</sup> To do this, the jet static temperature  $T_j$  has been set so that the ratio  $a_j/a_\infty$  of the local and ambient sound speeds is the same as in the helium jet, following Doty & McLaughlin.<sup>36</sup> The jets exhaust from straight-pipe nozzles at a static pressure matching the atmospheric pressure  $p_\infty = 10^5$  Pa. In addition, their mixing layers are initially in a laminar state, in agreement with measurements performed in supersonic jets at comparable Mach and Reynolds numbers.<sup>23</sup> The axial velocity profiles at the nozzle exit, shown in figure 1(a), are very similar to a Blasius boundary-layer mean velocity profile, whose thickness is equal to  $0.076r_0$  for the jets at  $Re_D = 50,000$  and to  $0.15r_0$  for the jet at  $Re_D = 12,500$ . These values are chosen to obtain momentum thickness  $\delta_\theta$  such that  $\delta_\theta/r_0 = 2/\sqrt{Re_D}$ , following an empirical relation introduced by Zaman<sup>37</sup> for initially-laminar subsonic jets. As a result, the boundary layers of the jet at  $Re_D = 12,500$  are thicker than those of the jets at  $Re_D = 50,000$ , as observed in figure 1(a). Moreover, in order to favor the transition of the shear-layers from a laminar to a turbulent state, small perturbations of the mixing layers are added inside the nozzle. These perturbations are solenoidal Gaussian vortex rings of random phases and amplitude, as proposed in Bogey et al.<sup>38</sup> The radial evolution of the root-mean-square (RMS) value of axial velocity fluctuations are plotted in figure 1(b). They are negligible from  $r = 0$  to  $r = 0.8r_0$ , in the jet inner potential core, and peak at  $0.03u_j$  near the nozzle lip. Consequently, the turbulence rates at the nozzle exit are low, and the jets can thus be considered as initially weakly disturbed.

**Table 1. Exhaust conditions for the three simulations.**

Simulation	$M_j$	$M_a$	$T_j/T_\infty$	$Re_D$
IsoRe12500	2.00	2.00	1.00	12,500
IsoRe50000	2.00	2.00	1.00	50,000
HotRe50000	1.50	2.06	1.87	50,000

### II.B. Numerical methods

The filtered compressible Navier-Stokes equations are solved in cylindrical coordinates  $(r, \theta, z)$  using an OpenMP based in-house solver. The convective and viscous flux are computed using the fourth-order, eleven-points, centered, low-dispersion finite difference schemes of Bogey & Bailly,<sup>39</sup> and a second-order, six-stage Runge-Kutta algorithm<sup>39</sup> is employed for time-integration. The method of Mohseni & Colonius<sup>40</sup> is used to remove the singularity on the jet axis, and the azimuthal derivatives near the jet axis are computed with fewer points than permitted by the grid in order to reduce the constraint on the time step.<sup>41</sup> More precisely, the effective number of points involved in the computations of the azimuthal derivatives progressively varies from 16 for points nearest to the jet axis to  $n_\theta = 256$  for  $r > 0.25r_0$ . At the end of each time-step, an eleven-point, sixth-order centered filter<sup>42</sup> is applied explicitly to the flow variables. This filtering operation allows for the suppression of grid-to-grid oscillations, as well as the relaxation of subgrid scale energy near the grid cut-off wavenumber. Since shock waves can be found in these highly compressible flows, a damping procedure using a dilatation-based shock detector and a second-order, optimized filter described in Bogey et al.<sup>42</sup> is used to remove Gibbs oscillations that can occur in the vicinity of shocks. Finally, in order to ensure that the computed sound field exits the computational domain without causing significant spurious reflexions, the radiation boundary conditions of Tam & Dong<sup>43</sup> are prescribed at its radial and axial boundaries. At

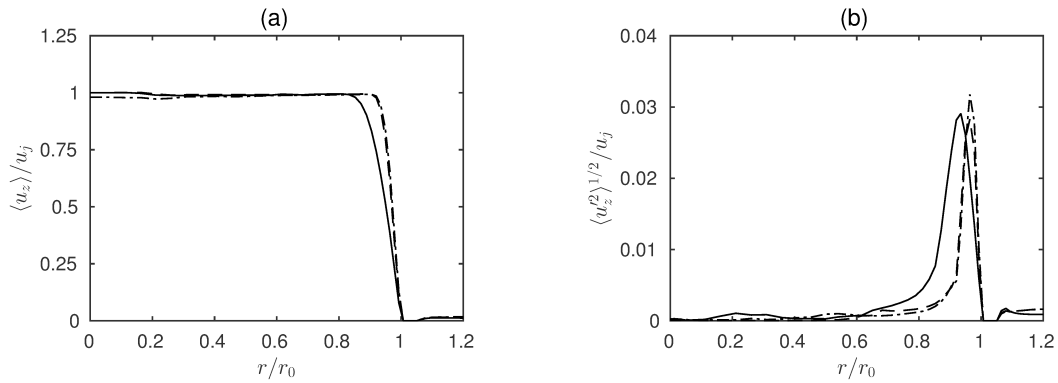


Figure 1. Radial profiles at the nozzle exit of (a) mean axial velocity and (b) RMS value of axial velocity fluctuations; **—** T1Re12500, **- - -** T1Re50000 and **- · - ·** T19Re50000.

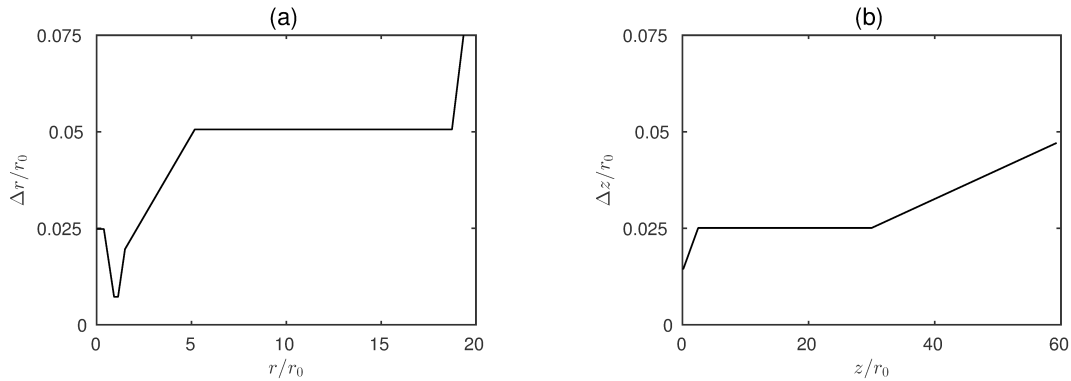


Figure 2. Evolutions of (a) radial and (b) axial mesh spacings.

the latter, they are associated with a sponge zone combining grid stretching and Laplacian filtering in order to damp flow perturbations before they reach the end of the computational domain.

### II.C. Computational parameters

The mesh grid used for the three simulations extends up to  $z = 60r_0$  in the axial direction, and out to  $r = 18r_0$  in the radial direction. It contains  $n_r = 526$ ,  $n_\theta = 256$  and  $n_z = 2294$  points in the radial, azimuthal and axial directions, respectively. The radial mesh spacing, represented in figure 2(a), is equal to  $0.025r_0$  on the jet centerline and is progressively decreased so that  $\Delta r = 0.00625r_0$  at  $r = r_0$ , in the shear-layers. Farther away from the jet centerline, the mesh spacing  $\Delta r$  progressively increases and reaches a maximum value of  $\Delta r_{max} = 0.05r_0$  for  $r \geq 5r_0$ , allowing a maximum Strouhal number  $St = fD/u_j$  of 5 for an acoustic wave discretized using four points per wavelength. The axial variations of the mesh spacing  $\Delta z$  are shown in figure 2(b). It is constant and equal to  $0.025r_0$  from  $z = 2.5r_0$ , near the nozzle exit, and down to  $z = 30r_0$ . Further downstream, it slowly increases but remains lower than  $\Delta r_{max} = 0.05r_0$ . The computations are carried out on 16-core nodes of Intel Xeon E5-2640 processors at 2.60 GHz. After an initial transient corresponding to roughly 50,000 iterations, the flow and sound fields are recorded during a simulation time  $t_s = 1000r_0/u_j$ , which necessitates the computation of 100,000 additional time steps. On the whole, each simulation requires roughly 40,000 CPU hours.

## III. Results

### III.A. Snapshots of the flow and acoustic fields

Snapshots of the jet flow and acoustic fields are shown in figure 3. In each case, vorticity norm is represented inside the jet flow, and pressure fluctuations outside. Near the nozzle, the flow field consists in an inner potential core surrounded by thin, parallel layers of vortical flow, which constitute the initially laminar

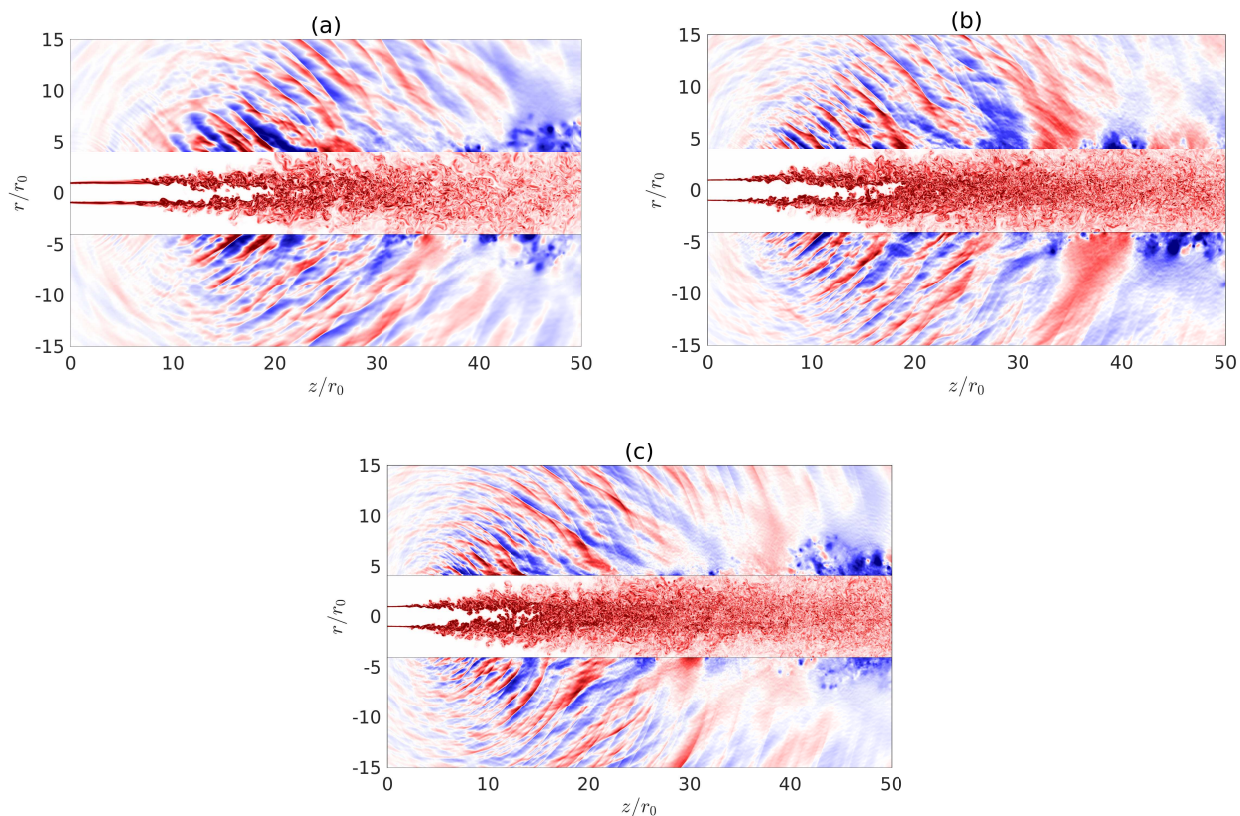


**Figure 3.** Instantaneous representations of the pressure fluctuations and the vorticity norm for (a) IsoRe12500, (b) IsoRe50000 and (c) HotRe50000. The color scales range from -3000 to 3000 Pa for pressure and up to  $4u_j/r_0$  for the vorticity norm, from blue to red.

mixing layers of the jets. Further downstream, a wider range of turbulent scales are found in the mixing layers, as a result of their transition from a laminar to a turbulent state. After this transition, the shear layers grow until they merge on the jet axis at  $z \simeq 20r_0$  and  $z \simeq 15r_0$  for the isothermal and hot jets, respectively. In the sound field, inclined, elongated wavefronts emerging from the jets are visible. These waves propagate in the downstream direction and are very similar to the ones observed in numerical simulations of supersonic jets emitting Mach waves.<sup>16,32,44</sup> Concerning the effects of Reynolds number, the sound fields of the jets at  $Re_D = 50,000$  contain more high frequency waves than the one radiated by the jet at  $Re_D = 12,500$ , as expected for an increase in Reynolds number.<sup>23,29</sup> Finally, for all of the jets, steep variations are discernible near the flow, suggesting the presence of shocks in the near acoustic field. These sharp gradients are mostly found at the edges of the wavefronts radiated from the jets shear layers, as in the simulation of Nichols et al.<sup>16</sup>

### III.B. Properties of the velocity fields

The axial profiles of the mean centerline axial velocity are plotted in figure 4(a) for the different jets. Shortly downstream of the nozzle exit, the centerline velocity remains very close to  $u_j$ , as long as the flow on the jet axis is potential. Slight variations of mean velocity are observed in the jet potential core, and are the footprints of weak shock cells that are formed downstream of the nozzle. Indeed, although the jet static pressure has been set equal to the ambient pressure, the presence of boundary layers inside the nozzle leads to the formation of shock cells. The amplitudes of these velocity variations, which are of the order of 5% of the jet velocity  $u_j$ , are weak, in agreement with measurements performed on the centerline of supersonic jets operated at ideally-expanded conditions.<sup>23</sup> Consequently, the present jets can be considered as nearly perfectly expanded. Further downstream of the nozzle exit, the mean centerline velocity begins to decay as a result of the intrusion of low-speed vortical flow on the jet axis as the potential core closes. More precisely, the axial position  $z_c$  where the potential core ends is defined according to the method of Lau et al.,<sup>45</sup> and is located at  $z_c = 15.7r_0$ ,  $14.4r_0$ , and  $11.2r_0$  for IsoRe12500, IsoRe50000 and HotRe50000, respectively. These

results can be compared to those obtained using an empirical formula introduced by Tam et al.,<sup>46</sup> written as

$$\frac{z_c}{2r_0} = 4.2 + 1.1M_j^2 + \left\{ \exp \left[ -3.2 \left( \frac{T_j}{T_\infty} - 1 \right) \right] - 1 \right\}, \quad (1)$$

yielding  $z_c = 17.2r_0$  and  $z_c = 11.5r_0$  for the isothermal and hot jets. Therefore, the potential core lengths in the present jets are slightly shorter than those predicted using equation (1). A possible explanation for this discrepancy is that the empirical formula (1) is based on measurements performed in high Reynolds number, initially turbulent jets, while the present jets are at moderate Reynolds numbers and are initially laminar. Indeed, it is known that supersonic jets with initially laminar mixing layers spread more rapidly, and have shorter potential cores than their turbulent counterparts.<sup>47</sup> Nevertheless, the present results are in good agreement with the evolution of  $z_c$  predicted using the model of Tam et al.<sup>46</sup> In particular, the shorter potential core length observed in the case of the hot jet can be attributed, from (1), to temperature as well as to Mach number effects. Finally, the evolution of the centerline Mach number is shown in figure 4(b). In the case of the hot jet at  $M_j = 1.5$ , the results are in very good agreement with the experimental measurements of Papamoschou & Debiasi<sup>31</sup> for a helium jet at comparable exhaust conditions.

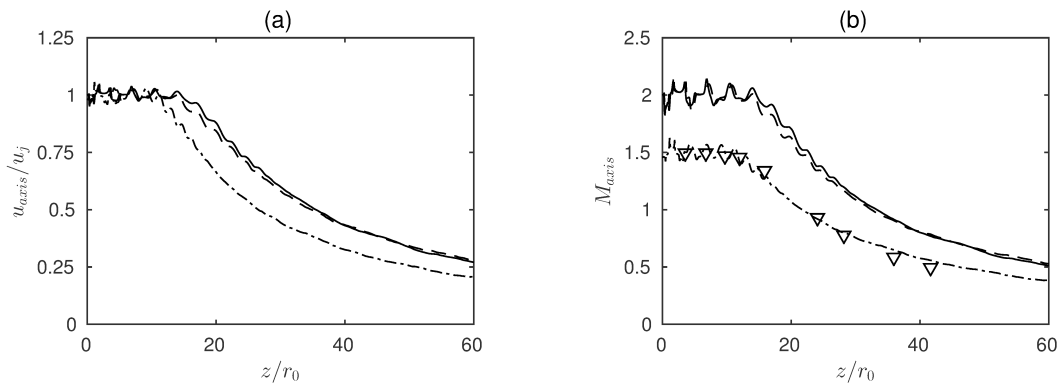


Figure 4. Axial variations of (a) mean centerline velocity and (b) mean axial Mach number for IsoRe12500, IsoRe50000 and HotRe50000. The triangles in (b) indicate experimental measurements by Papamoschou & Debiasi<sup>31</sup>.

In order to characterize the development of the turbulent flow, the variations of the RMS values of axial velocity fluctuations are shown in figure 5. The RMS values at  $r = 0$ , represented in figure 5(a), are negligible near the nozzle exit and increase rapidly further downstream, when the potential core closes. They reach a peak just after the end of the potential core, at  $z = 22.9r_0$ ,  $23.5r_0$ , and  $16.4r_0$  for IsoRe12500, IsoRe50000 and HotRe50000, and slowly decrease afterward as a result of the jet spreading. Inside the shear layers, the maximum RMS values of velocity fluctuations, represented in figure 5(b), are close to 3% of the jet exhaust velocity at  $z = 0$ , as expected from figure 1(b). Further downstream, they increase very rapidly and reach a maximum of  $0.20u_j$  and  $0.22u_j$  for the isothermal and hot jets. These peaks are similar to the ones observed in simulations of initially-laminar subsonic jets,<sup>48</sup> and can be attributed to the merging of initial vortices occurring during the shear layer transition from a laminar to a turbulent state. For the jets at  $Re_D = 50,000$ , these maxima are located very close to the nozzle exit, at  $z = 3.9r_0$  and  $2.7r_0$  for IsoRe50000 and HotRe50000. For IsoRe12500, the peak velocity fluctuations are located further downstream, at  $z = 8.5r_0$ , which results from the latter transition of the shear layers to a turbulent state in this case, as visible in figure 3(a).

### III.C. Properties of the near acoustic field

#### III.C.1. Mean and spectral properties of the sound field

The Overall Sound Pressure Levels (OASPL), computed at a distance  $r = 15r_0$  from the jet centerline, are represented in figure 6(a). In all cases, a peak is obtained. For IsoRe50000, for example, the noise level is 20 dB higher at the location of peak noise emission than at  $z = 0$ , which suggests that the main sources of sound are highly directive. The sound pressure levels for the two isothermal jets are nearly identical. In particular, they peak at 153.9 dB and 153.5 dB at  $Re_D = 12,500$  and  $Re_D = 50,000$ . As a comparison, Freund et al.<sup>32</sup> obtained a peak sound pressure level of 154 dB at  $r = 15r_0$  in their Direct Numerical

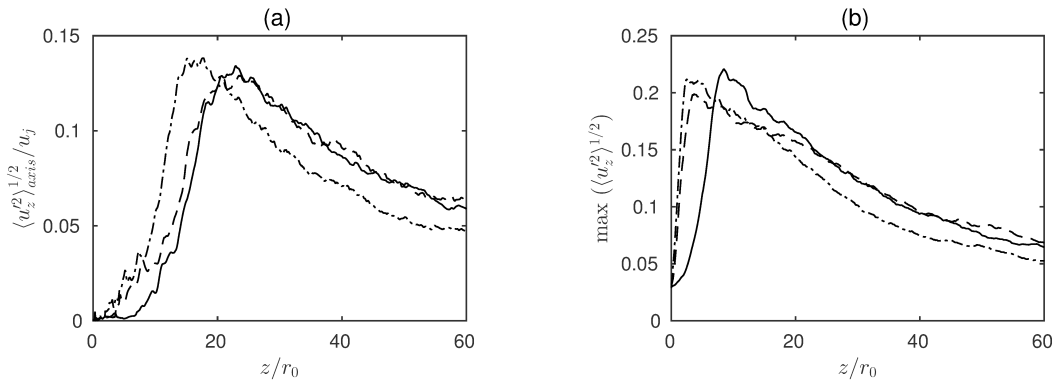


Figure 5. Axial variations of (a) the RMS value of centerline axial velocity fluctuations and (b) the maximum value of the RMS value of velocity fluctuations for the jets — IsoRe12500, - - - IsoRe50000, and - · - · HotRe50000.

Simulation of a jet at an acoustic Mach number of 2, and at  $T_j/T_\infty = 1.12$  and  $Re_D = 4,000$ . Furthermore, the position of peak noise is found at  $z = 21r_0$  for IsoRe50000, but slightly downstream, at  $z = 26r_0$  for IsoRe12500. This difference can be related to the location of peak velocity fluctuations, which is also located farther from the nozzle in the case of the lower Reynolds number in figure 5(b). Finally, the sound levels radiated by the hot jet peak at a value of 151.5 dB, at  $z = 19r_0$ . Consequently, for an acoustic Mach number remaining close to 2, the isothermal jets are louder than the hot jet, in agreement with measurements by Tanna et al.<sup>49</sup>

The Power Spectrum Densities (PSD) of the pressure fluctuations computed at the locations of maximum sound pressure levels at  $r = 15r_0$  are shown in figure 6(b). They peak at Strouhal numbers of 0.3, 0.4 and 0.5 for IsoRe12500, IsoRe50000 and HotRe50000, respectively. After the peak, the pressure levels decrease at a regular slope whose value is close to -20 dB per decade, in agreement with measurements performed in the near and far acoustic fields of supersonic jets in the direction of peak noise emission.<sup>4,50,51</sup> Finally, the spectra have very similar shapes, which supports the fact that the sound generation mechanisms at play are the same in the three jets considered.

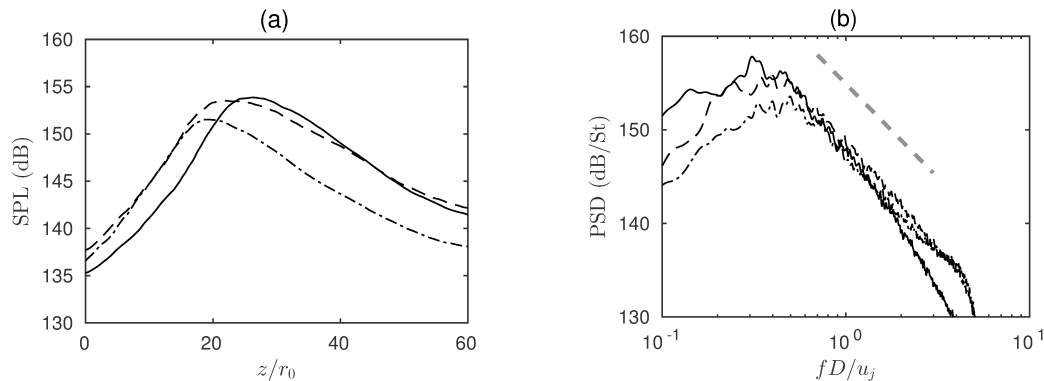


Figure 6. Representation of (a) the axial variations of OASPL at  $r = 15r_0$  and (b) the power spectrum density of pressure fluctuations at the position of peak pressure fluctuations at  $r = 15r_0$ , for — IsoRe12500, - - - IsoRe50000, and - · - · HotRe50000. The dashed gray line indicates a slope of -20 dB per decade.

### III.C.2. Shocks in the near acoustic field

In figure 3, steep variations are found at the edges of the wavefronts radiated from the jets, which suggests that shocks are present in the near acoustic field. In the past, several metrics have been proposed to characterize the presence of shocks in the sound field of supersonic jets.<sup>1,2,5,52</sup> In particular, Ffowcs-Williams et al.<sup>5</sup> have correlated the perception of crackle to the occurrence of strong overpressures in the acoustic signals. These pronounced peaks lead to a positive asymmetry of the statistical distribution of pressure fluctuations,

which can be characterized by computing its skewness factor  $S(p)$ , defined as

$$S(p) = \frac{\langle p'^3 \rangle}{\langle p'^2 \rangle^{3/2}}. \quad (2)$$

These authors postulated that crackle is distinctly heard for values of  $S(p)$  higher than 0.4, but absent when  $S(p)$  is lower than 0.3. In the present study, the skewness factors of the pressure fluctuations computed at  $r = 15r_0$  for the three jets are represented in figure 7(a). Unfortunately, they are poorly converged, which is reflected in the noisy rendering of the data. Despite this, they take significant positive values from, approximately,  $z = 10r_0$  down to  $z = 30r_0$ , which corresponds to the region where steep wavefronts are observed in figure 3. More precisely, the skewness values are found between 0.3 and 0.4 at the locations of peak noise levels, which is slightly lower than the threshold of 0.4 introduced by Ffowcs Williams et al.<sup>5</sup>

Another commonly-used metric to assess the presence of crackle is the skewness factor of the pressure time derivative  $S(dp/dt)$ .<sup>52,53</sup> Indeed, positive values of  $S(dp/dt)$  indicate the prevalence of fast compressions in the pressure waveforms, which is also a manifestation of the presence of shocks. Similarly, another possibility is to compute the skewness factor of the dilatation  $\Theta$ , which is defined as the divergence of the velocity field. Indeed, the presence of shocks leads to a negative asymmetry of the dilatation, and to negative values of its skewness factor  $S(\Theta)$  as highlighted, for instance, by Lee et al.<sup>54</sup> in simulations of decaying compressible isotropic turbulence. In addition, it is noteworthy that in the case of isentropic, linear acoustic waves,  $\Theta$  and  $dp/dt$  are related by

$$\Theta = -\frac{1}{\rho_\infty a_\infty^2} \frac{dp}{dt}, \quad (3)$$

yielding  $S(\Theta) = -S(dp/dt)$ . The skewness factor of the dilatation at  $r = 15r_0$ , shown in figure 7(b), is significantly negative from, approximately,  $z = 15r_0$  down to  $z = 40r_0$ . The lowest values are respectively -3.4 for the jet at  $Re_D = 12,500$  and -2.6 for the jets at  $Re_D = 50,000$ , and they are reached at  $z = 28r_0$ , which is slightly downstream of the location of maximum pressure fluctuations. Therefore, from figure 7(a,b), it can be concluded that significant values of the skewness of pressure fluctuations and dilatation are present at  $r = 15r_0$ , which reveals a pronounced asymmetry of the acoustic waves at this location. The skewness is strong in the direction of peak sound emission, but less marked upstream and downstream of the peak, where sound pressure levels are lower.

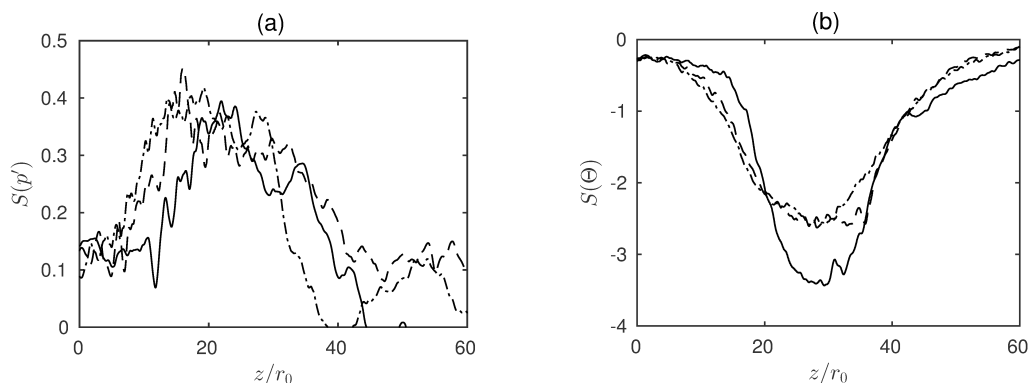


**Figure 7.** Representation at  $r = 15r_0$  of the skewness factor of (a) the pressure fluctuations and (b) the dilatation for the jets — IsoRe12500, - - - IsoRe50000, and - · - · HotRe50000.

In order to investigate the variations of skewness in the near acoustic field, the skewness factors of the pressure and dilatation fields calculated over the whole section  $(r, z)$  are represented in figure 8 for IsoRe12500. For the pressure fluctuations, in figure 8(a), positive values are noted in the immediate vicinity of the turbulent flow, and they are highest close to the peak of sound emission. Moreover, it decreases down to values lower than 0.2 upstream and downstream of the maximum. Furthermore, regarding the evolution of  $S(p)$  with increasing distance from the jet, no clear trend can be distinguished in figure 8(a). In figure 8(b), a distinctive peak of negative values of  $S(\Theta)$  emerges close to the maximum of sound emission. It originates from the immediate vicinity of the turbulent flow, between  $r = 2r_0$  and  $r = 5r_0$ . Far from the peak of sound emission,  $S(\Theta)$  is close to 0, indicating that sharp gradients are absent from the waveforms. Finally, the skewness of the dilatation appears to decrease with the propagation distance, which suggests the presence of nonlinear propagation effects.

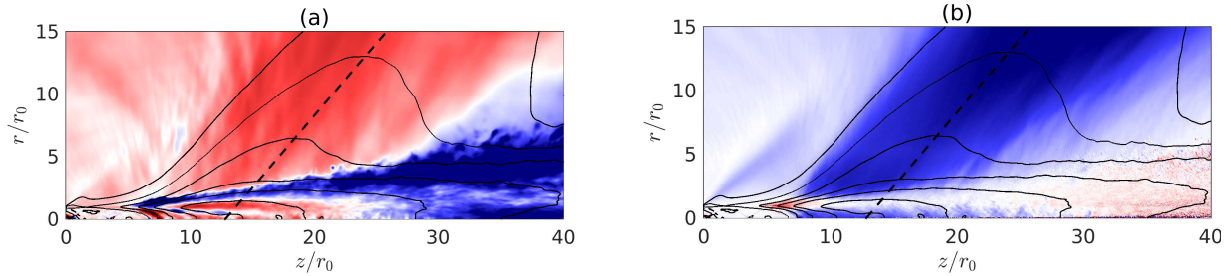


**Figure 8.** Representation of the skewness factor of (a) pressure fluctuations and (b) dilatation for IsoRe12500. The solid lines indicate the contours of sound pressure levels ranging from 150 dB to 175 dB and separated by 5 dB. The dashed line indicates the position of maximum sound pressure level, and the color scales range from -0.6 to 0.6 in (a) and from -3 to 3 in (b), from blue to red.

In order to further investigate the evolution of the asymmetry of the sound waves with propagation distance, the skewness of the pressure and dilatation fields have been computed on the line where noise levels are maximum. As represented in figure 8, this line is oriented at a shallow angle from the jet axis. For the three jets, the skewness of the pressure fluctuations in figure 9(a) starts at a value lower than 0.2 at  $r = 3r_0$ , and progressively increases with radial distance. More precisely, it reaches values of 0.31, 0.36 and 0.41 at  $r = 15r_0$  for IsoRe12500, IsoRe50000 and HotRe50000. In figure 9(b), the skewness of the dilatation is close to -2 at  $r = 3r_0$  for the three jets, and diminish when the radial distance is increased. This decrease can be attributed to the effects of nonlinear steepening, as well as to shock coalescence,<sup>18,19</sup> and is much more pronounced for the jet at  $Re_D = 12,500$ . This suggests that nonlinear propagation effects are more important for the lower Reynolds number jet. However, further investigations are needed to clarify this point.

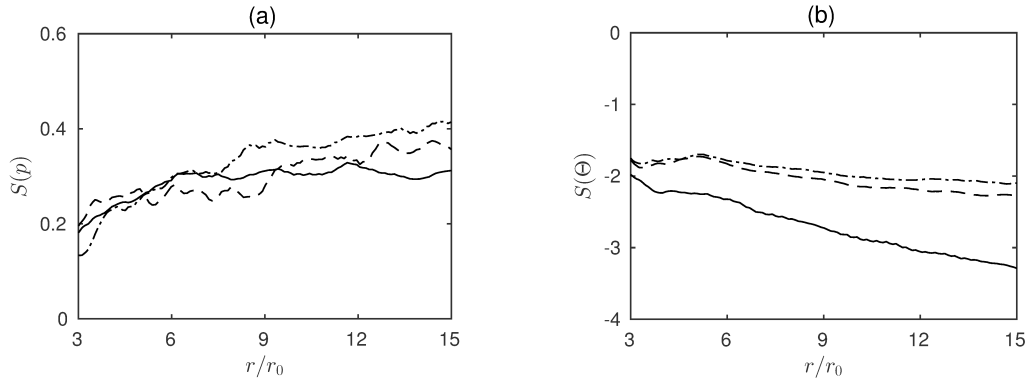


**Figure 9.** Evolution along the line of maximum sound emission of (a)  $S(p)$  and (b)  $S(\Theta)$  for — IsoRe12500, - - - IsoRe50000, and - · - · HotRe50000.

An important conclusion of the results of figure 9 is that the skewed character of the pressure fluctuations and of the dilatation are well pronounced in the very near acoustic field. Assuming this asymmetry results from the presence of shocks, this is consistent with previous conclusions that steepened waves at the origin of crackle are formed, at least partly, by a source mechanism located inside the turbulent flow.<sup>2,16,18</sup> In order to illustrate this point, three sample signals of pressure fluctuations and dilatation are shown in figure 10 for IsoRe12500. They are recorded at three positions located at  $r = 5r_0$ ,  $10r_0$  and  $15r_0$  on the line array depicted in figure 8. For comparison, they are normalized by their RMS values and represented as a function of  $t + \tau$ , where  $\tau = 0$  at  $r = 5r_0$ ,  $\tau = 13.8r_0/u_j$  at  $r = 10r_0$ , and  $\tau = 26.4r_0/u_j$  at  $r = 15r_0$ . The time delay  $\tau$  accounts for the propagation time between the reference position  $r = 5r_0$  and a given measurement point, and is determined from the peak of cross-correlations between the two signals. In figure 10(a) the most salient features of the pressure waveforms recorded at  $r = 15r_0$  are distinguishable at  $r = 5r_0$ , in the near vicinity of the turbulent flow. Notably, steep shock-like structures are consistently found at, for instance,  $(t + \tau)u_j/r_0 = 4, 8, 12,$  and  $24$  at the three radial locations. This is even more striking for the dilatation in figure 10(b), where distinctive negative peaks, indicating strong compressions, are observed at the same corrected times. Therefore, it is likely that a significant portion of the shocks at  $r = 15r_0$  are already present

at  $r = 5r_0$ , in the immediate vicinity of the turbulent flow, and that they propagate along the line array. This observation supports the conclusion that the shocks are mainly the result of a source mechanism inside the jets. One notable exception concerns the shock at  $(t + \tau)u_j/r_0 = 20$ . While it is distinctly seen in the waveforms at  $r = 15r_0$  and  $r = 10r_0$ , it is not in the signal at  $r = 5r_0$ . This shock is most probably formed by the coalescence of at least two smaller shocks, as highlighted in the studies of Buchta & Freund,<sup>18</sup> or Fiévet et al.<sup>19</sup> Finally, a slight decrease of some of the negative dilatation peaks with increasing radial distance can be noted in figure 10(b) as, for example, at  $(t + \tau)u_j/r_0 = 4, 8$  and  $12$ , which suggests a steepening of the wavefronts. This steepening could be the consequence of cumulative nonlinear propagation effects. However, since the propagation distances at play are very short, these effects remain slight.

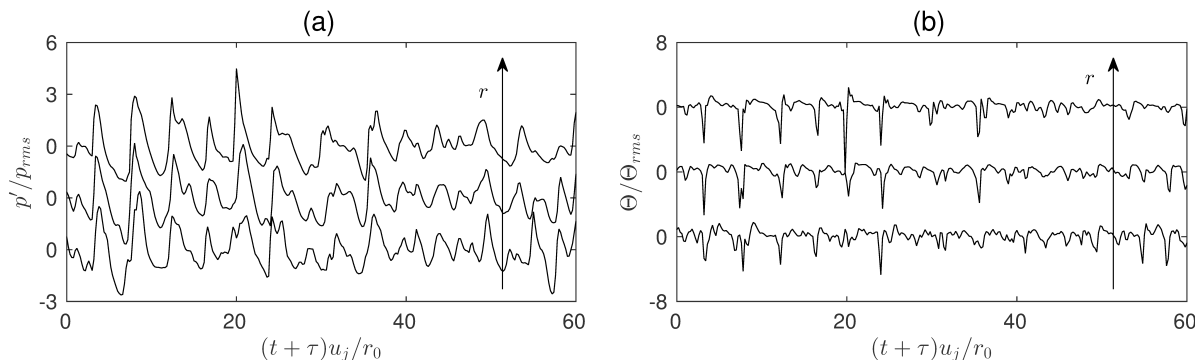


**Figure 10.** Evolution of (a) pressure fluctuations  $p'$  and (b) dilatation  $\Theta$  for the jet IsoRe12500 at, from top to bottom,  $r = 5r_0$ ,  $r = 10r_0$ , and  $r = 15r_0$  along the line of maximum sound emission. The pressure fluctuations and the dilatation are normalized by their standard deviation.

In order to trace back the steep nature of the sound field and to study its properties as close as possible to the turbulent flow, the pressure fluctuations have been recorded on a conical antenna aligned with the jet axis and spanning the entire azimuthal extent of the jet. This antenna, represented in figure 11, is located at  $r = 1.4r_0$  at  $z = 0$  and spreads with an angle of  $11^\circ$  whose value has been chosen to closely match the jet development. From the nozzle exit down to  $z \simeq 5r_0$ , the pressure fluctuations close to this antenna consist of high-frequency, low-amplitude waves. They are generated just upstream of the peak of RMS velocity fluctuations in figure 5(b), where the shear layers of the jets are still in a laminar state. Further downstream, from approximately  $z = 5r_0$  down to  $z = 15r_0$ , the waves emerging from the shear layers are stronger, and sharp pressure gradients are present at their edges. Notably, intense, steepened wavefronts cross the conical antenna at  $z \simeq 8r_0$ ,  $z \simeq 12r_0$  and  $z \simeq 15r_0$ , for instance. Finally, for  $z$  greater than  $20r_0$ , approximately, the pressure fluctuations are dominated by lower-frequency waves, whose steepened aspect is less marked. For comparison, the axial variations of sound pressure levels on the conical antenna are represented in figure 12(a). They peak at  $z = 15.0r_0$ ,  $7.8r_0$  and  $5.1r_0$  for IsoRe12500, IsoRe50000 and HotRe50000, which is close to the locations where steepened waves are observed in figure 11 for IsoRe50000. In addition, the skewness factor of the dilatation, represented in figure 12(b), starts very close to 0 at  $z = 0$ , which indicates that the noise produced in the near vicinity of the nozzle exit is not significantly skewed, confirming the observations in figure 11. Further downstream, it rapidly decreases down to strongly negative levels, and remains slightly lower than -2 over several jet diameters. In particular, it can be noted that  $S(\Theta)$  is always lower than -2 at the axial locations of peak pressure levels. These negative values of skewness can be related to the sharp pressure variation distinguished in figure 11.

### III.D. Conditional averages

In order to investigate the main characteristics of the steepened waves observed in the near vicinity of the jets, it can be useful to study their properties independently from the rest of the waveform. To do so, the signals of pressure fluctuations recorded on the conical antenna in figure 10 are split in time intervals of length  $5r_0/u_j$ . For each of these intervals, the peak of pressure fluctuations is localized, and the time  $t_{\text{trig}}$  and azimuthal angle  $\theta_{\text{trig}}$  where this maximum occurs are used as triggers in a conditional averaging procedure. This procedure consists in synchronizing the pressure fluctuations in time and space, according to  $t_{\text{trig}}$  and  $\theta_{\text{trig}}$ , respectively, before performing an ensemble average at the end of which only the strongest, generic features of the synchronized events are preserved.

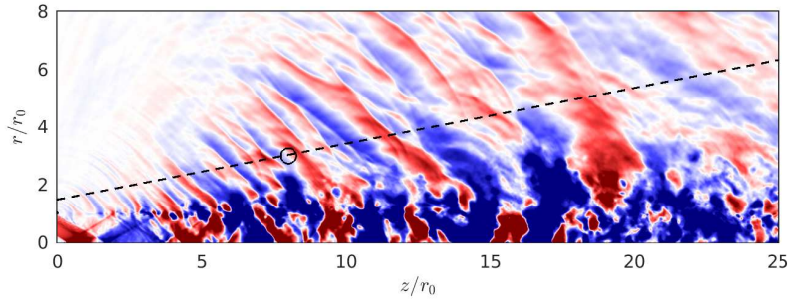


Figure 11. Snapshots of the pressure fluctuations for IsoRe50000. The near-field conical antenna is represented in dashed lines, and the black circle indicates the position of maximum sound pressure levels on the antenna. The color scale ranges from -10,000 Pa to 10,000 Pa, from blue to red.

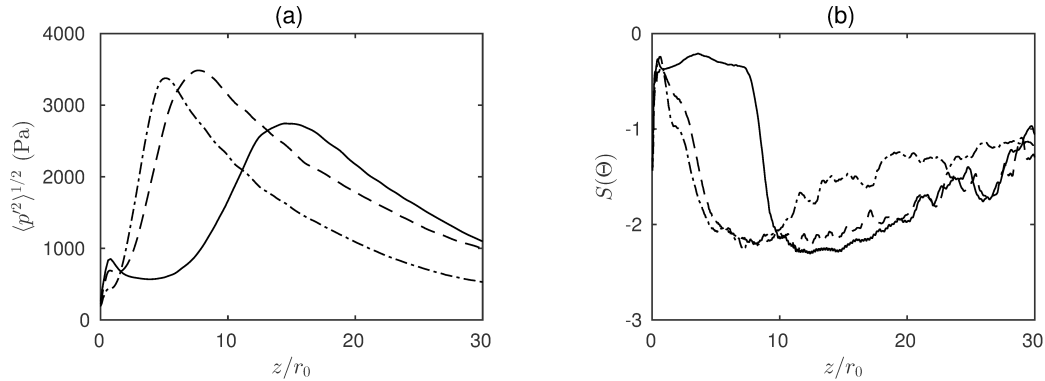
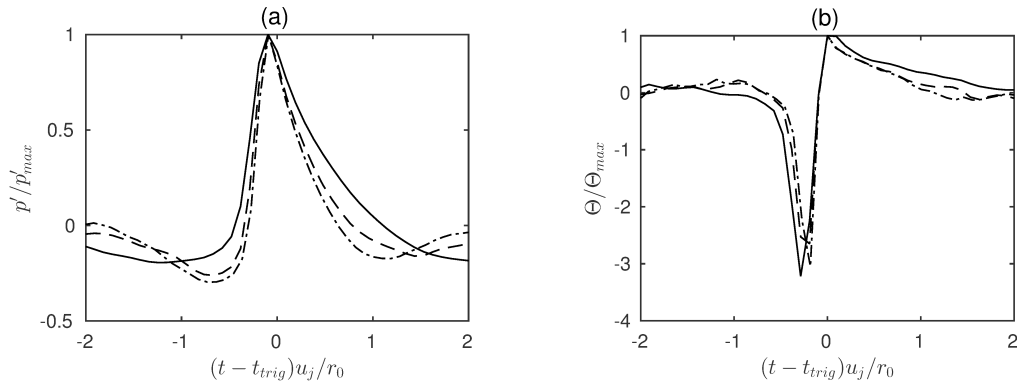


Figure 12. Variations along the near-field antenna of (a) the RMS value of pressure fluctuations and (b) the skewness factor of dilatation for  $\text{—}$  IsoRe12500,  $\text{-- --}$  IsoRe50000, and  $\text{- \cdot - \cdot}$  HotRe50000.

The conditional averages are applied to the pressure and dilatation signals recorded on the conical antenna at the positions of maximum pressure fluctuations. The resulting ensemble averaged pressure and dilatation, computed using approximately 200 events, are shown in figure 13. They are normalized by their maximum value, and plotted as a function of the nondimensionalized time delay  $(t - t_{\text{trig}})u_j/r_0$ , to facilitate the comparison between the different cases. In figure 13(a), the pressure waveforms resulting from the conditional averages all share the same distinctive shape. More particularly, a compression phase during which the pressure rapidly rises to its peak value is observed for  $t \leq t_{\text{trig}}$ . After this compression, a gradual expansion allows the relaxation of the pressure down to slightly negative levels. Similarly, in figure 13(b), a strong negative peak of dilatation is found just before  $t = t_{\text{trig}}$ , and is followed shortly after by a much less pronounced positive one. This observation can be related to the asymmetry of the pressure waveforms in figure 13(a). Indeed, the dominance of the negative dilatation peaks, when compared to the maxima in figure 13(b) indicates that the time scales associated with the compression phase in figure 13(a) are much shorter than that of the expansion phase. As a result, the distinctive signature usually associated with crackle noise is clearly recovered in the present conditional averages, which confirms the adequacy of this method, based on the detection of strong pressure events, for investigating the properties of shocks in the jet near field. Finally, the time scales  $\tau_p$  associated with the conditionally-averaged pressure signals can be estimated by computing the full width at half maximum of the pressure peaks in figure 13(a), yielding  $\tau_p = 0.62r_0/u_j$ ,  $\tau_p = 0.45r_0/u_j$ , and  $\tau_p = 0.38r_0/u_j$  for IsoRe12500, IsoRe50000, and HotRe50000. These values are comparable to the eddy turnover time  $r_0/u_j$ , which is representative of the largest turbulent scales inside the flow. However,  $\tau_p$  is slightly longer for the jet at  $Re_D = 12,500$ , suggesting that the shape of the waveforms can be affected by variation of Reynolds numbers.

Is is also possible to synchronize the two-dimensional fields based on the same trigger events used to compute the conditional averages in figure 13. In particular, such conditional averages are useful since they provide a way to establish correlations between the flow and acoustic fields. In the present study, the flow and sound fields are synchronized according to the maxima of the pressure fluctuations signals recorded on the conical antenna. The objective is to examine the process by which strong, steepened waves, like



**Figure 13.** Conditionally-averaged (a) pressure and (b) dilatation signals normalized by their maximum values at locations of maximum pressure fluctuations for  $\text{---}$  IsoRe12500,  $\text{- - -}$  IsoRe50000, and  $\text{- \cdot - \cdot}$  HotRe50000.

the ones depicted in figure 11, are generated from the jet flow. In jets radiating Mach waves, it is known that the majority of sound intensity is contained within the low-order azimuthal modes.<sup>44</sup> Therefore, the present conditional averages are performed on three-dimensional reconstructions of the flow and sound fields involving only the first five azimuthal Fourier modes.

Plane views of the conditionally averaged fields obtained for the three jets considered are represented in figure 14. More precisely, the pressure fluctuations are shown at times  $t = t_s$ ,  $t = t_s + 4r_0/u_j$ ,  $t = t_s + 8r_0/u_j$ , and  $t = t_s + 12r_0/u_j$ . The reference time  $t_s$  is defined as  $t_s = t_{\text{trig}} - r_{\text{trig}}/a_\infty$ , where  $r_{\text{trig}}$  is the radial position where the trigger signal is acquired on the conical antenna. In this definition, the duration  $r_{\text{trig}}/a_\infty$  accounts for the propagation from  $r = 0$  up to the location  $r = r_{\text{trig}}$  where shocks are detected. As a result, the instant  $t = t_s$  corresponds to the moment when the wave is generated inside the jet flow. Contours of conditionally-averaged vorticity norm are also superimposed on figure 14. In order to remove the component resulting from the mean shear, the time-averaged vorticity have been subtracted before computing the averages. Finally, in order to visualize the jet structure, three contours of conditionally-averaged axial velocity are shown. The innermost contour corresponds to  $u_z = 0.95u_j$  and defines the edge of the potential core, while the second one corresponds to the sonic line  $u_z = a_\infty$ . Finally, the third velocity contour, defined as  $u_z = 0.05u_j$  represents the outer boundary of the jet flow. At  $t = t_s$ , a strong pressure wave is seen emerging from the jet shear layers at  $z \simeq 10r_0$  for IsoRe12500,  $z \simeq 6r_0$  for IsoRe50000 and  $z \simeq 4r_0$  for HotRe50000. At the inner tip of this wave, a vorticity excess is visible in the high speed side of the shear layers. This vorticity spot has an elliptical shape, and its radial extent spans the supersonic side of the shear layers, from the edge of the potential core up to the sonic line. Meanwhile, a region of strong positive pressure can be seen in the shear layers, just upstream of the vorticity spot. At  $t = t_s + 4r_0/u_j$ , the vorticity is found downstream from its initial position and remains connected to the pressure wave, which rises more frankly from the shear layers. In addition, steep pressure gradients are discernible at the edge of the wavefront, which is in agreement with the shapes of the time traces of figure 13(a). Interestingly, despite its steepened aspect, the structure of this wave reminds that of wavepackets distinguished in a previous study of Mach wave radiation.<sup>26</sup> At  $t = t_s + 8r_0/u_j$ , and  $t = t_s + 12r_0/u_j$ , the pressure wave propagates in the jet aft quadrant, while the vorticity spot continues its motion and eventually disappears. The time evolution of the axial location of peak vorticity  $z_\omega$  is plotted in figure 15(a). The fairly linear aspect of these curves indicates nearly constant convection speeds  $u_c$  whose values can be estimated by a linear fit of the data. This estimation yields convection velocities of  $u_c = 0.79u_j$ ,  $0.81u_j$  and  $0.69u_j$  for IsoRe12500, IsoRe50000 and HotRe50000, in agreement with the values of eddy-convection speeds measured in supersonic jets at similar Mach numbers.<sup>23</sup> Notably, they are much higher than the ambient speed of sound, which is consistent with the generation of Mach waves. In order to interpret the present results, it is assumed, following Hussain<sup>55</sup> and Zaman & Hussain,<sup>34</sup> that the vorticity excess in the conditional averages constitutes a mean representation of the coherent structures developing in the jet shear layers. As visible in figure 14, the pressure field associated with such coherent structures consists, in average, of a local pressure deficit followed by a marked pressure excess. As sketched by Ribner,<sup>56</sup> this wavepacket-like pressure disturbance acts on the surrounding medium as a wavy wall: It induces a local compression-expansion process which, when convected at a supersonic speed, propagates in the far acoustic field as sound. While most models of the Mach wave phenomenon rely on a linear description of this wavy wall mechanism,<sup>24,26,57</sup> it is likely that the linear assumption might not hold when the perturbation induced

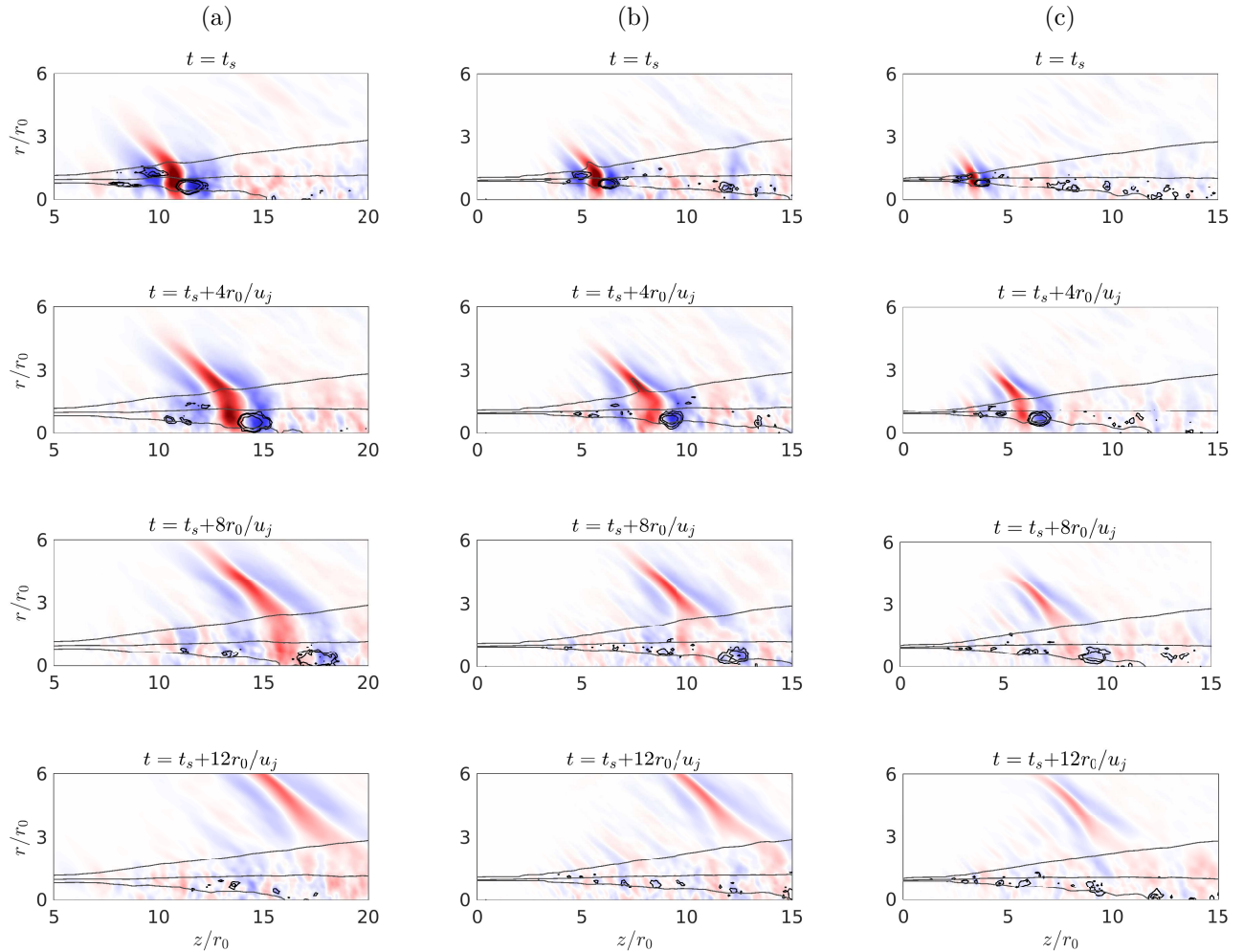


**Figure 14.** Time evolution of conditionally-averaged pressure and vorticity fluctuations for (a) IsoRe12500, (b) IsoRe50000 and (c) HotRe50000; — contours of vorticity fluctuations corresponding to  $0.15u_j/r_0$ ,  $0.30u_j/r_0$ , and  $0.60u_j/r_0$ , — contour of conditionally-averaged axial velocity for the values  $0.95u_j$ ,  $a_\infty$ , and  $0.05u_j$ . The color scale for the pressure fluctuations ranges from -10,000 to 10,000 Pa, from blue to red.

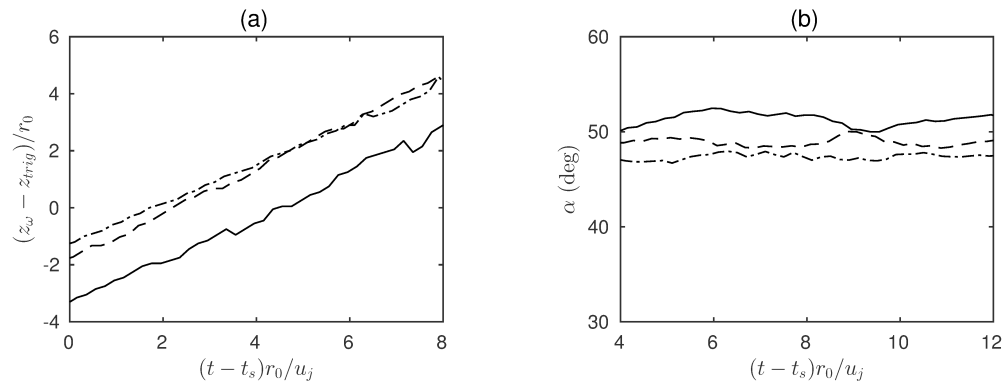


**Figure 15.** Time evolution of (a) the axial position  $z_\omega$  of the maximum of coherent vorticity and (b) the propagation angle  $\alpha$  for — IsoRe12500, - - - IsoRe50000, and - · - · HotRe50000.

by flow perturbations are strong enough. As pointed out by Buchta,<sup>17</sup> for instance, such nonlinearities could lead to the generation of steepened waves, as the ones in figure 11. To confirm that the steepened waves in figure 14 are indeed related to the supersonic convection of coherent structures, their orientation angles can be compared to those obtained from the mean convection velocities  $u_c$  from figure 15(a) using the relation

$$\cos \alpha = \frac{a_\infty}{u_c}. \quad (4)$$

To do so, the angles  $\alpha$  are estimated by computing the direction of the local pressure gradient with respect to the jet axis at the location of minimum conditionally-averaged dilatation, that is, at the location of sharpest pressure gradients. The resulting angles in figure 15(b), are nearly constant, and equal to 51, 49, and 47 degrees for IsoRe12500, IsoRe50000 and HotRe50000. These values fall within less than 3 degrees from the propagation angle estimated from (4), which are equal to 51, 52 and 45 degrees for IsoRe12500, IsoRe50000 and HotRe50000. It strongly suggests that the steepened waves in figure 14 are linked, in some way, to the supersonic convection of coherent structures inside the jet shear layers. Finally, the lower normalized convection speed for the hot jet is in agreement with previous observations that the ratio  $u_c/u_j$  decreases with increasing static temperature.<sup>58,59</sup> Interestingly, this decrease of the convection velocity can be related to the observation in figure 7(a) that the peak sound pressure levels produced by the hot jet are lower than those of the isothermal jets. Indeed, since the three jets have the same acoustic Mach number, a decrease in convection speed is expected to lead to a less pronounced convective amplification, resulting in a decreased efficiency of the Mach wave radiation mechanism for the hot jet. However, despite the lower sound pressure levels, there appears to be no significant effect of increasing temperature on the shape of the conditionally-averaged waveforms in figure 13.

## IV. Conclusion

In this paper, the mechanisms leading to the formation of shocks in the near acoustic fields of supersonic jets are investigated by considering numerical simulations of isothermal and heated supersonic jets at an acoustic Mach number of 2. The computations include two simulations of isothermal jets at Reynolds numbers of 12,500 and 50,000, as well as one simulation of a heated jet at a Reynolds number of 50,000. Steep, asymmetric pressure waves are observed in the jet near fields, leading to positive and negative levels of the skewness factors of pressure and dilatation, respectively. The asymmetry of the sound field is significant in the immediate vicinity of the turbulent flow, suggesting that the steepened aspect of the waves is present at the time of their generation. This hypothesis is confirmed by the analysis of pressure time traces recorded at different stations along a linear antenna located in the direction of peak noise emission. Indeed, a significant portion of the shocks observed at  $r = 15r_0$  are also present at  $r = 5r_0$ , very close to the jets. Therefore, it is suggested, following previous investigators,<sup>2,5,16,18</sup> that the steep nature of the waves is, to a large extent, the consequence of a source mechanism located inside the turbulent flow. In order to investigate this source mechanism, conditional averages of the flow and sound fields are computed to isolate the strongest events from the pressure signals, with the aim of investigating their generic properties. In these conditional averages, straight, steepened wavefronts are seen emerging from the jet shear layers. Inside the flow, these wavefronts are connected to regions of high vorticity that are convected at supersonic speeds. Since the convection velocities of these vorticity spots are consistent with the measured propagation angles, a possible interpretation of the conditional averages is that the steepened wavefronts observed near the turbulent flow constitute a nonlinear variety of Mach waves. Indeed, while Mach wave radiation is generally described as a linear phenomenon, it is likely that in the case of strong flow disturbances, nonlinear effects could lead to a steepening of the wavefronts at the source. However, further investigations are needed to confirm this hypothesis and, in particular, to define at what point a given flow perturbation becomes strong enough to give rise to the generation of shocks. In addition, a more detailed description of nonlinear propagation effects is needed in order to understand how the present waves propagate in the far acoustic field. In particular, for the jet at  $Re_D = 12,500$ , a marked steepening of the sound field is noted with increasing distance from the jet, and has been attributed to nonlinear propagation effects. These effects appear to be much less pronounced for  $Re_D = 50,000$ , which motivates further investigations.

## Acknowledgments

This work was granted access to the HPC resources of FLMSN (Fédération Lyonnaise de Modélisation et Sciences Numériques), partner of EQUIPEX EQUIP@MESO, and of the resources of IDRIS (Institut du Développement et des Ressources en Informatique Scientifique) under the allocation 2017-2a0204 made by GENCI (Grand Equipement National de Calcul Intensif). It was performed within the framework of the Labex CeLyA of Université de Lyon, operated by the French National Research Agency (Grant No. ANR-10-LABX-0060/ANR-11-IDEX-0007).

## References

- <sup>1</sup>Baars, W. and Tinney, C. E., “Shock-structures in the acoustic field of a Mach 3 jet with crackle,” *Journal of Sound and Vibration*, Vol. 333, 2014, pp. 2539–2553.
- <sup>2</sup>Krothapalli, A., Venkatakrishnan, L., and Lourenco, L., “Crackle: A dominant component of supersonic jet mixing noise,” *AIAA paper 2000-2024*, 2000.
- <sup>3</sup>Laufer, J., Schlinker, R., and Kaplan, R., “Experiments on supersonic jet noise,” *AIAA Journal*, Vol. 14, No. 4, April 1976.
- <sup>4</sup>Schlinker, R., Liljenberg, S., Polak, D., Post, K., and Chipman, C., “Supersonic jet noise source characteristics and propagation: engine and model scale,” *AIAA paper 2007-3623*, 2007.
- <sup>5</sup>Ffowcs Williams, J. E., Simson, J., and Virchis, V. J., “‘Crackle’: an annoying component of jet noise,” *Journal of Fluid Mechanics*, Vol. 71, 1975, pp. 251–271.
- <sup>6</sup>Morfey, C. L. and Howell, G. P., “Nonlinear propagation of aircraft noise in the atmosphere,” *AIAA Journal*, Vol. 19, No. 8, 1980, pp. 986–992.
- <sup>7</sup>Gee, K. L., Sparrow, V. W., James, M. M., Downing, M. J., Hobbs, C. M., Gabrielson, T. B., and Atchley, A. A., “Measurements and prediction of noise propagation from a high-power jet aircraft,” *AIAA paper 2006-2531*, 2006.
- <sup>8</sup>Reichman, B. O., Gee, K. L., Neilsen, T. B., Swift, S. H., Wall, A. T., Gallagher, H. L., Downing, J. M., and James, M. M., “Acoustic shock formation in noise propagation during ground run-up operations of military aircraft,” *AIAA Paper 2017-4043*, 2017.
- <sup>9</sup>de Cacqueray, N. and Bogey, C., “Noise of an overexpanded Mach 3.3 jet: non-linear propagation effects and correlations with flow,” *International Journal of Aeroacoustics*, Vol. 13, No. 7-8, 2014, pp. 607–632.
- <sup>10</sup>Petitjean, B., *On the nonlinearities in the noise radiated from high-speed model jets*, Ph.D. thesis, The Pennsylvania State University, 2006.
- <sup>11</sup>Baars, W., Tinney, C. E., and Hamilton, M. F., “On cumulative nonlinear acoustic waveform distortions from high-speed jets,” *Journal of Fluid Mechanics*, Vol. 749, 2014, pp. 331–366.
- <sup>12</sup>Baars, W., Tinney, C. E., and Hamilton, M. F., “Piecewise-spreading regime model for calculating effective Gol’dberg numbers for supersonic jet noise,” *AIAA Journal*, Vol. 54, No. 9, 2016, pp. 2833–2841.
- <sup>13</sup>Murray, N. E. and Lyons, G. W., “On the convection velocity of source events related to supersonic jet crackle,” *Journal of Fluid Mechanics*, Vol. 793, 2016, pp. 477–503.
- <sup>14</sup>Rossmann, T., Mungal, M., and Hanson, T., “Evolution and growth of large-scale structures in high compressibility mixing layers,” *Journal of Turbulence*, Vol. 9, No. 3, 2001, pp. 1–16.
- <sup>15</sup>Nichols, J. W., Lele, S. K., and Spyropoulos, J. T., “The source of crackle noise in heated supersonic jets,” *AIAA paper 2013-2197*, 2013.
- <sup>16</sup>Nichols, J. W., Lele, S. K., Ham, F. E., Martens, S., and Spyropoulos, J. T., “Crackle noise in heated supersonic jets,” *Journal of Engineering for Gas Turbines and Power*, Vol. 135, No. 5, 2013, pp. 051202.
- <sup>17</sup>Buchta, D. A., *Crackle noise from high-speed free-shear-flow turbulence*, Ph.D. thesis, University of Illinois at Urbana-Champaign, 2016.
- <sup>18</sup>Buchta, D. A. and Freund, J. B., “The near-field pressure radiated by planar high-speed free-shear-flow turbulence,” *Journal of Fluid Mechanics*, Vol. 832, 2017, pp. 383–408.
- <sup>19</sup>Fiévet, R., Tinney, C. E., Baars, W. J., and Hamilton, M. F., “Coalescence in the sound field of a laboratory-scale supersonic jet,” *AIAA Journal*, Vol. 54, No. 1, January 2016, pp. 254–265.
- <sup>20</sup>Martens, S., Spyropoulos, J. T., and Nagel, Z., “The effects of chevrons on crackle-engine and scale model results,” *Proceedings of the ASME Turbo Expo, GT2011-46417*, 2011.
- <sup>21</sup>Tam, C. K. W., “Supersonic Jet Noise,” *Annual Review of Fluid Mechanics*, Vol. 27, No. 1, 1995, pp. 17–43.
- <sup>22</sup>Tam, C. K. W., Viswanathan, K., Ahuja, K. K., and Panda, J., “The sources of jet noise: experimental evidence,” *Journal of Fluid Mechanics*, Vol. 615, 2008, pp. 253292.
- <sup>23</sup>Troutt, T. R. and McLaughlin, D. K., “Experiments on the flow and acoustic properties of a moderate-Reynolds-number supersonic jet,” *Journal of Fluid Mechanics*, Vol. 116, 1982, pp. 123–156.
- <sup>24</sup>Tam, C. K. W. and Burton, D. E., “Sound generated by instability waves of supersonic flows. Part 2. Axisymmetric jets,” *Journal of Fluid Mechanics*, Vol. 138, 1984, pp. 273295.
- <sup>25</sup>Tam, C. K. W., Chen, P., and Seiner, J. M., “Relationship between instability waves and noise from high-speed jets,” *AIAA Journal*, Vol. 30, No. 7, July 1992, pp. 1747–1752.
- <sup>26</sup>Sinha, A., Rodriguez, D., Brès, G., and Colonius, T., “Wavepacket models for supersonic jet noise,” *Journal of Fluid Mechanics*, Vol. 742, 2014, pp. 71–95.

- <sup>27</sup>Mohseni, K., Colonius, T., and Freund, J. B., “An evaluation of linear instability waves as sources of sound in a supersonic turbulent jet,” *Physics of Fluids*, Vol. 14, 2000, pp. 787–795.
- <sup>28</sup>McLaughlin, D. K., Morisson, G. L., and Troutt, T. R., “Reynolds number dependance in supersonic jet noise,” *AIAA Journal*, Vol. 15, No. 4, 1977, pp. 526–533.
- <sup>29</sup>Bogey, C. and Bailly, C., “Investigation of downstream and sideline subsonic jet noise using Large Eddy Simulation,” *Theoretical and Computational Fluid Dynamics*, Vol. 20, No. 1, Feb 2006, pp. 23–40.
- <sup>30</sup>Petitjean, B., Viswanathan, K., and McLaughlin, D., “Acoustic pressure waveforms measured in high speed jet noise experiencing nonlinear propagation,” *International Journal of Aeroacoustics*, Vol. 5, No. 2, 2006, pp. 193–215.
- <sup>31</sup>Papamoschou, D. and Debiasi, M., “Directional suppression of noise from a high-speed jet,” *AIAA Journal*, Vol. 39, No. 3, March 2001.
- <sup>32</sup>Freund, J. B., Lele, S. K., and Moin, P., “Numerical simulations of a Mach 1.92 turbulent jet and its sound field,” *AIAA Journal*, Vol. 38, No. 11, November 2000, pp. 2023–2031.
- <sup>33</sup>Lau, J. C., Fisher, M. J., and Fuchs, H. V., “The intrinsic structure of turbulent jets,” *Journal of Sound and Vibration*, Vol. 22, No. 4, 1972, pp. 379–706.
- <sup>34</sup>Zaman, K. B. M. Q. and Hussain, A. K. M. F., “Natural large-scale structures in the axisymmetric mixing layer,” *Journal of Fluid Mechanics*, Vol. 138, 1984, pp. 325–351.
- <sup>35</sup>Brown, G., L. and Thomas, A. S. W., “Large structure in the turbulent boundary layer,” *Physics of Fluids*, Vol. 20, 1977, pp. 243–252.
- <sup>36</sup>Doty, M. J. and McLaughlin, D. K., “Acoustic and mean flow measurements of high-speed, helium-air mixture jets,” *International Journal of Aeroacoustics*, Vol. 2, No. 2, 2003, pp. 293–334.
- <sup>37</sup>Zaman, K. B. M. Q., “Effect of initial condition on subsonic jet noise,” *AIAA Journal*, Vol. 23, No. 9, 1985, pp. 1370–1373.
- <sup>38</sup>Bogey, C., Marsden, O., and Bailly, C., “Large-Eddy Simulation of the flow and acoustic fields of a Reynolds number 105 subsonic jet with tripped exit boundary layers,” *Physics of Fluids*, Vol. 23, No. 3, 2011, pp. 025104.
- <sup>39</sup>Bogey, C. and Bailly, C., “A family of low dispersive and low dissipative explicit schemes for noise computation,” *Journal of Computational Physics*, Vol. 194, No. 1, 2004, pp. 194–214.
- <sup>40</sup>Mohseni, K. and Colonius, “Numerical treatment of polar coordinate singularities,” *Journal of Computational Physics*, Vol. 157, No. 10, 2002, pp. 3593–3600.
- <sup>41</sup>Bogey, C., Marsden, O., and Bailly, C., “Finite differences for coarse azimuthal discretization and for reduction of effective resolution near origin of cylindrical flow equations,” *Journal of Computational Physics*, Vol. 230, 2011, pp. 1134–1146.
- <sup>42</sup>Bogey, C., de Cacqueray, N., and Bailly, C., “A shock-capturing methodology based on adaptive spatial filtering for high-order non-linear computations,” *Journal of Computational Physics*, Vol. 228, 2009, pp. 1447–1465.
- <sup>43</sup>Tam, C. K. W. and Dong, Z., “Radiation and outflow boundary conditions for direct computation of acoustic and flow disturbances in a nonuniform mean flow,” *Journal of Computational Acoustics*, Vol. 4, No. 2, 1996, pp. 175–201.
- <sup>44</sup>de Cacqueray, N., Bogey, C., and Bailly, C., “Investigation of a High-Mach-Number Overexpanded Jet Using Large-Eddy Simulation,” *AIAA Journal*, Vol. 49, No. 10, Oct 2011, pp. 2171–2182.
- <sup>45</sup>Lau, J. C., Morris, P. J., and Fisher, M. J., “Measurements in subsonic and supersonic free jets using a laser velocimeter,” *Journal of Fluid Mechanics*, Vol. 93, No. 1, 1979, pp. 1–27.
- <sup>46</sup>Tam, C. K. W., A., J. J., and Seiner, J. M., “A multiple-scales model of the shock-cell structure of imperfectly expanded supersonic jets,” *Journal of Fluid Mechanics*, Vol. 153, 1985, pp. 123–149.
- <sup>47</sup>Nonomura, T., Oyama, A., Fujii, K., Morihira, K., Pichon, G., and Terakado, D., “Effects of disturbed nozzle-exit boundary layers on acoustic waves from ideally-expanded supersonic jets,” *AIAA paper 2016-2936*, 2016.
- <sup>48</sup>Bogey, C., Marsden, O., and Bailly, C., “Influence of initial turbulence level on the flow and sound fields of a subsonic jet at a diameter-based Reynolds number of 100,000,” *Journal of Fluid Mechanics*, Vol. 701, 2012, pp. 352–385.
- <sup>49</sup>Tanna, H. K., Dean, P. D., and Fisher, M. J., “The influence of temperature on shock-free supersonic jet noise,” *Journal of Sound and Vibration*, Vol. 39, No. 4, 1975, pp. 429–460.
- <sup>50</sup>Petitjean, B. and McLaughlin, D., “Experiments on the nonlinear propagation of noise from supersonic jets,” *AIAA paper 2003-3127*, 2003.
- <sup>51</sup>Greska, B., Krothapalli, A., Horne, W. C., and Burnside, N., “A near-field study of high temperature supersonic jets,” *AIAA paper 2008-3026*, 2008.
- <sup>52</sup>McInerny, S. A., “Launch vehicle acoustics part 2: statistics of the time domain data,” *Journal of Aircraft*, Vol. 33, No. 3, 1977, pp. 518–523.
- <sup>53</sup>Gee, K. L., Swift, S. H., Sparrow, V. W., Plotkin, K. J., and Downing, M. J., “On the potential limitations of conventional sound metrics in quantifying perception of nonlinearly propagated noise,” *The Journal of the Acoustical Society of America*, Vol. 121, No. 1, 2007, pp. EL1–EL7.
- <sup>54</sup>Lee, S., Lele, S. K., and Moin, P., “Eddy shocklets in decaying compressible turbulence,” *Physics of Fluids*, Vol. 657, No. 3, 1991, pp. 657–664.
- <sup>55</sup>Hussain, A. K. M. F., “Coherent structures and turbulence,” *Journal of Fluid Mechanics*, Vol. 173, 1986, pp. 303–356.
- <sup>56</sup>Ribner, H. S., “Eddy Mach wave noise from a simplified model of a supersonic mixing layer,” Tech. Rep. UTIAS Technical note No. 146, UTIAS, 1969.
- <sup>57</sup>Tam, C. K. W. and Morris, P., “The radiation of sound by the instability waves of a compressible plane turbulent shear layer,” *Journal of Fluid Mechanics*, Vol. 98, No. 2, 1980, pp. 349381.
- <sup>58</sup>Ecker, T. E., Lowe, K. T., and Ng, W. F., “Eddy convection in developing heated supersonic jets,” *AIAA Journal*, Vol. 53, No. 11, November 2015, pp. 3305–3315.
- <sup>59</sup>Gojon, R., Baier, F., Gutmark, E., and Mihaescu, M., “Temperature effects on the aerodynamic and acoustic fields of a rectangular supersonic jet,” *AIAA paper 2017-0002*, 2017.